Grism-based pulse shaper for line-by-line control of more than 600 optical frequency comb lines

M. S. Kirchner[1,2,*] and S. A. Diddams[2,3]

[1]*Department of Physics, University of Colorado, 2000 Colorado Avenue, Boulder, Colorado 80309, USA*

[2]*National Institute of Standards and Technology, 325 Broadway, MS 847, Boulder, Colorado 80305, USA*

[3]*e-mail: sdiddams@boulder.nist.gov*

**Corresponding author: mkirchne@boulder.nist.gov*

Received June 2, 2010; accepted August 9, 2010;
posted August 31, 2010 (Doc. ID 129487); published September 27, 2010

We construct a line-by-line pulse shaper using a grism (grating plus prism) dispersive element, which provides constant angular dispersion over 13.4 THz centered at ~311 THz (965 nm). When combined with a dual-mask liquid crystal modulator, this grism-based shaper is capable of line-by-line amplitude and phase control of over 600 modes of a 21 GHz stabilized optical frequency comb.

OCIS codes: 320.5540, 070.6120, 050.0050.

Fourier-domain femtosecond pulse shaping has evolved from manipulating the phase and amplitude of groups of frequency comb modes [1–3] to addressing the individual components of a frequency comb [4–8]. Line-by-line pulse shaping allows full control over the amplitude and phase of a pulse and is a route to optical arbitrary waveform generation. The complexity of the waveform that can be generated increases with the bandwidth of frequencies that can be manipulated. Different geometries exist to achieve this line-by-line control [5–8], but one of the simplest and easiest to implement is a grating-based free-space pulse shaper with a spatial light modulator (SLM) in the focal plane (Fig. 1). Typical grating-based shapers have shown line-by-line control over ~100 individual comb modes [5,6], limited by the number of modulator pixels or comb modes available and the nonuniform angular dispersion of the grating in the pulse shaper [6]. This nonuniform angular dispersion causes the comb modes to be unevenly spaced in the focal plane of the shaper, making it difficult to match each pixel of the modulator with only one frequency comb mode. The work presented here uses a custom grism (grating plus prism) to make the angular dispersion in the shaper sufficiently uniform to the point where more than 600 frequency comb modes can be lined up one to one with the pixels of a spatial light modulator.

Typical free-space pulse shapers use a grating and a lens to disperse and focus frequency comb modes to a focal plane, each mode separated by $\Delta x = f\Delta\theta$, as shown in Fig. 1. It is straightforward to solve for Δx or $\Delta\theta$ using the grating equation for a given frequency comb spacing, grating, lens, and input angle. Additionally, one can calculate how close each comb mode is to the center of its intended SLM pixel by integrating the mode spacing minus the pixel pitch (in our case, 100 μm). Figure 2(a) shows the mode spacing Δx as a function of mode number for a 21 GHz comb centered at 965 nm for a line-by-line shaper constructed with an 800 mm lens and a 1200 lines/mm grating, with the center mode spacing matched to the 100 μm pixel pitch of the SLM used in this work.

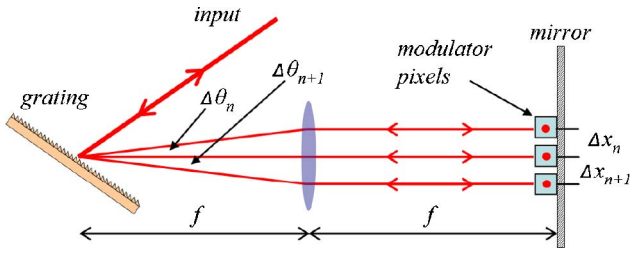

Fig. 1. (Color online) Grating-based line-by-line pulse shaper. Each comb mode is independently controlled by one or more pixels of a modulator. The modes are then recombined with an identical lens-grating system or with retroreflection.

Because the mode spacing changes across the spectrum, the comb modes "walk off" the centers of the pixels [Fig. 2(b)]. This "walk-off" is cumulative, so the pixel centers and the mode centers quickly become misaligned. Outside the center region of good alignment, the pixels and modes alias rapidly and line-by-line control is not possible in the one pixel per comb mode setup. Using two pixels or more per comb mode can mitigate this issue; however, this decreases the maximum number of modes available for control.

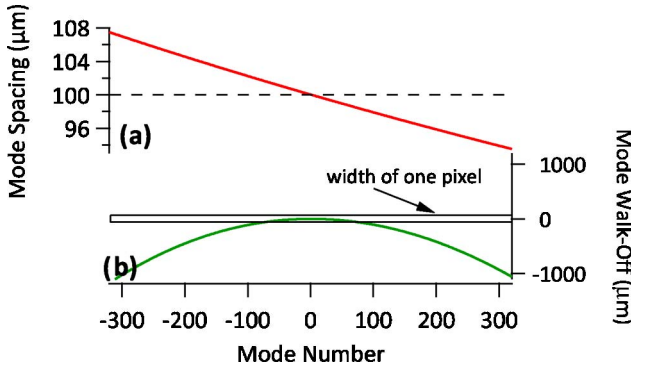

Fig. 2. (Color online) (a) Mode spacing (Δx) as a function of mode number with mode 0 at 965 nm. The mode spacing is close to 100 μm/mode only in the center. (b) Integrated residual mode walk-off shows that fewer than 200 modes stay aligned with the correct SLM pixel. Only about 100 modes are close enough to the center of the pixel to avoid spatial overlap with neighboring pixels.

To increase the number of modes we can control in the one pixel per mode geometry, we have to alter the properties of the dispersive element so that the dispersion is flat across the region of interest, satisfying the condition $\delta^2\theta_{\text{out}}/\delta\lambda^2 = 0$. This is accomplished by inserting a prism on top of the grating, as shown in Fig. 3. The tilted dielectric interface at the prism–air surface maps the disperion of the grating onto an inverse sine function from Snell's law, and, for the right design parameters, the nonlinear angular dispersion becomes linear. Past work has combined gratings and prisms to linearize the dispersion of an astronomical spectrometer [9], but in the ultrafast optics field, grisms have been used most commonly for pulse compression [10,11].

Solving for the output angle of a grism as a function of wavelength or frequency allows one to find $\Delta\theta$ between comb modes spaced by a given repetition frequency. For the geometry shown in Fig. 3, the output angle of a grism is

$$\theta_{\text{out}} = \sin^{-1}\left[n(\lambda)\sin\left(\sin^{-1}\left[\frac{m\lambda}{n(\lambda)d} - \sin\left(\sin^{-1}\left[\frac{1}{n(\lambda)}\sin(\theta_{\text{in}} - \alpha)\right] + \alpha\right)\right] - \alpha\right)\right] + \alpha, \quad (1)$$

where θ_{in} and θ_{out} are the input and output angles as defined in Fig. 3, α is the apex angle of the prism, $n(\lambda)$ is the index of the prism as a function of wavelength, $m = 1$ is the diffraction order, d is the groove spacing, and λ is the wavelength of the comb mode.

To design our grism, we attempt to set $\delta^2\theta_{\text{out}}/\delta\lambda^2 = 0$ while keeping $\Delta x = f\Delta\theta \approx 100$ μm. We found that this can be accomplished for a 21 GHz comb centered at 965 nm using an equilateral fused silica prism, a 1200 lines/mm grating, a 750 mm focal length achromatic lens, and $\theta_{\text{in}} = -2.1°$. This solution also operates the grating near Littrow so the grating efficiency is maximized. We had some flexibility in choosing our comb repetition rate, because we are using a cavity filtered 1 GHz comb and can select repetition rates in integer multiples of 1 GHz [12]. However, this solution is not unique, and, in general, one can find a solution with off-the-shelf parts for many comb repetition rates and center wavelengths. The theoretical solution showed a mode spacing near 100 μm/mode and much less integrated walk-off than

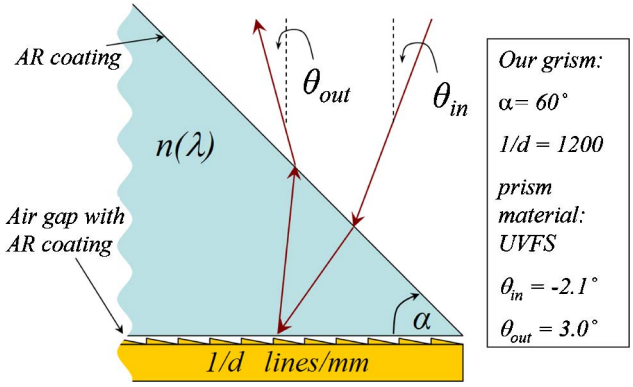

Fig. 3. (Color online) Reflection grism geometry. The angled dielectric interface of the prism serves to alter the dispersion of the grating. Input and output angles are measured clockwise with respect to grating normal.

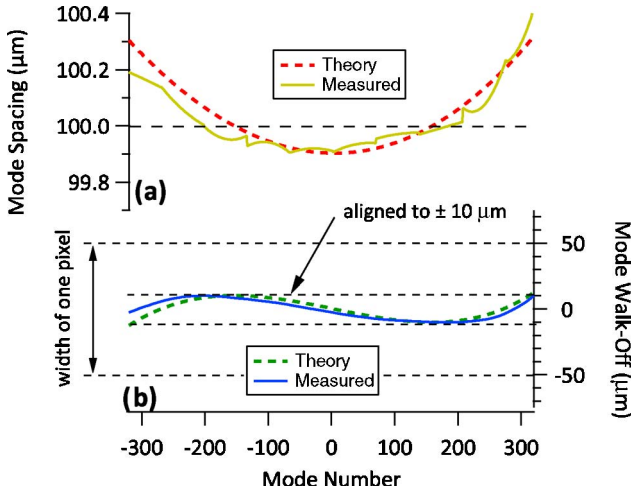

Fig. 4. (Color online) (a) Mode spacing (Δx) as a function of mode number with the theory (dashed) and measurement (solid) showing good agreement. The mode spacing is close to 100 μm/mode over the entire aperture of the SLM (640 pixels). (b) Integrated mode walk-off shows that over 600 modes are within 10 μm of pixel center. Theory (dashed curves) and measurement (solid curves) again show good agreement.

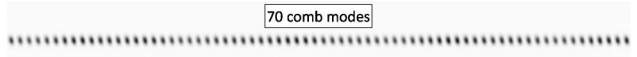

Fig. 5. Example CCD image showing 70 comb modes spaced by 100 μm.

the grating-based shaper, with more than 600 modes within 10 μm of pixel center (Fig. 4).

To measure the mode spacing in our grism-based pulse shaper, we replaced the grating element in the shaper with the grism described above. The grism showed a single-pass efficiency of 80%. A CCD camera was placed in the focal plane of the pulse shaper to image the comb modes and measure the mode spacing (Fig. 5). A line-out from each image was fitted with an array of Gaussians to extract the mode spacing. The measured mode spacing was compared to the theoretical model to find the current input angle. With minor adjustments to the input angle, the grism shaper showed the correct mode spacing in the focal plane.

A series of approximately ten images was taken by translating the CCD camera to cover the entire dispersed frequency comb (spanning over 6 cm), and the mode spacings were extracted from each image. The ten mode spacing measurements were then stitched together and compared with our theoretical model (Fig. 4). The integrated walk-off from the measured mode spacings shows that there are over 600 comb modes within ± 10 μm of pixel center [Fig. 4(b)], as predicted by theory.

These CCD measurements also allowed us to extract the beam waist of comb modes in different areas of the spectrum. Beam waist is important because it determines how much cross talk there will be between neighboring pixels. The nonzero optical path length through the pixels (~3 mm) constrains the minimum intensity beam waist at the pixel surface farthest from the focus to 30 μm, corresponding to an intensity beam waist of 22 μm at the focus. We measured a waist of 25 μm at the focus across most of the comb (Fig. 6). At this

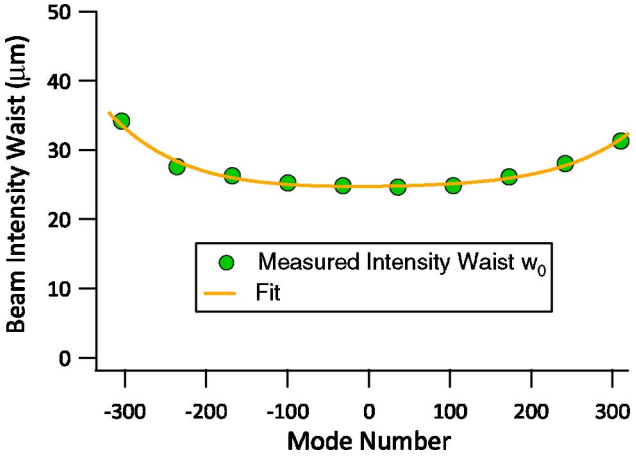

Fig. 6. (Color online) Intensity beam waist measured across the aperture of the SLM shows beam waists near 25 μm for most of the comb.

measured waist, 98% of the power is contained within the correct pixel for perfect alignment, decreasing to 96.7% for 10 μm of misalignment. The measured beam waist expands in the wings of the spectra due to chromatic aberration in the imaging system, but even at the largest beam waist, 93% and 91% of the power is contained in the correct pixel for perfect alignment and 10 μm of misalignment, respectively.

After characterizing the mode spacing and beam waist, we inserted a 640 pixel amplitude and phase SLM with 100 μm pixel pitch into the focal plane of the line-by-line pulse shaper. To achieve good pixel alignment over the entire aperture of the SLM, we first attenuate every other pixel on the SLM and look at the comb on an optical spectrum analyzer (OSA). If there is good alignment between the pixels and comb modes, the trace on the OSA will look like a frequency comb with double the comb mode spacing. Coarse alignment can be obtained by translating the SLM with a translation stage or translating the comb modes with a mirror, and fine adjustments can be made by tuning the comb repetition rate slightly. The well-aligned case is shown in Fig. 7.

Good alignment of the comb to the SLM pixels is established across the entire 13.4 THz bandwidth ($\Delta\lambda = 41$ nm). This is verified in the measurement of the "off" state modes, which show attenuation of 10–20 dB. This could be improved through better calibration of the SLM. There is some attenuation of the "on" state modes, especially in the lower end of the spectrum, possibly due to an increase in beam waist in this region.

To our knowledge, this 13.4 THz is the largest bandwidth of optical frequency that has been addressed in

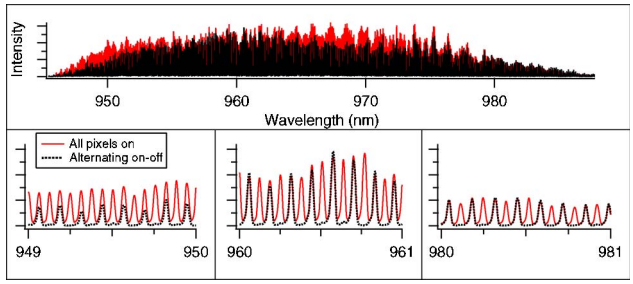

Fig. 7. (Color online) Top, OSA traces showing the shaped frequency comb on a linear scale with all pixels in the "on" state (solid red curve) and pixels alternating between "on" and "off" (dashed black curves). Bottom, zoomed sections of the top traces showing that the alignment of the comb modes with the SLM pixels is good across the whole bandwidth of the frequency comb.

a line-by-line manner. The expansion in both the number of modes and the bandwidth controlled makes more complex optical and microwave arbitrary waveforms possible. Furthermore, this grism technique should be similarly effective in pulse shapers at 1550 nm or in other dispersive systems where constant angular dispersion is desireable.

We thank Steve Kane, Jeff Squier, and Charles Durfee for their helpful discussions and Tara Fortier for providing the stabilized 1 GHz Ti:sapphire laser.

References

1. J. P. Heritage, A. M. Weiner, and R. N. Thurston, Opt. Lett. **10**, 609 (1985).
2. M. M. Wefers and K. A. Nelson, Opt. Lett. **18**, 2032 (1993).
3. A. M. Weiner, Prog. Quantum Electron. **19**, 161 (1995).
4. Z. Jiang, D. S. Seo, D. E. Leaird, and A. M. Weiner, Opt. Lett. **30**, 1557 (2005).
5. Z. Jiang, C. Huang, D. E. Leaird, and A. M. Weiner, Nat. Photon. **1**, 463 (2007).
6. M. S. Kirchner, T. M. Fortier, D. Braje, A. M. Weiner, L. Hollbert, S. A. Diddams, *Ultrafast Phenomena XVI* (Springer, 2009).
7. N. K. Fontaine, R. P. Scott, J. Cao, A. Karalar, W. Jiang, K. Okamoto, J. P. Heritage, B. H. Kolner, and S. J. B. Yoo, Opt. Lett. **32**, 865 (2007).
8. V. R. Supradeepa, Ch.-B. Huang, D. E. Leaird, and A. M. Weiner, Opt. Express **16**, 11878 (2008).
9. W. A. Traub, J. Opt. Soc. Am. A **7**, 1779 (1990).
10. S. Kane and J. Squier, J. Opt. Soc. Am. B **14**, 661 (1997).
11. E. A. Gibson, D. M. Gaudiosi, H. C. Kapteyn, R. Jimenez, S. Kane, R. Huff, C. Durfee, and J. Squier, Opt. Lett. **31**, 3363 (2006).
12. M. S. Kirchner, D. A. Braje, T. M. Fortier, A. M. Weiner, L. Hollberg, and S. A. Diddams, Opt. Lett. **34**, 872 (2009).